

Model of collective behavior using bio-plausible visual cues

Diego Castro,^{1,2,*} Franck Ruffier,¹ and Christophe Eloy²

¹*Aix Marseille Université, CNRS, ISM, Marseille, France*

²*Aix Marseille Université, CNRS, Centrale Marseille, IRPHE, Marseille, France*

(Dated: May 12, 2023)

Animal collective behavior is often modeled with self-propelled particles, assuming that each individual has perfect knowledge of its neighbors' position and orientation. In reality, this information may not be directly accessible however, especially when neighbors are hidden from view. To address this limitation, we propose a model that uses bio-plausible visual cues as the sole sensory input. Our model successfully reproduces three classical collective behaviors: swarming, schooling, and milling. These findings provide new insights into animal collective behavior and offers a potential solution for coordinating artificial swarms with vision.

Collective animal behavior is a common phenomenon in nature, from the mesmerizing movements of starling murmurations to the coordinated motion of cattle herds [1–4]. Since the pioneering work of Vicsek [5], researchers have been interested in understanding how models based on simple rules followed by each individual can give rise to these complex collective behaviors [6–8].

Models of collective behavior are generally based on self-propelled particles, where individual particles with an intrinsic speed orient themselves based on three fundamental rules: alignment, attraction, and avoidance (often referred to as the “3A” rules) [9–11]. These models have been successful in capturing different collective behaviors, such as swarming –no orientational order–, schooling –high orientational order–, and milling –the group swirls in a circular pattern– [12–15].

In self-propelled particle models, the rules of attraction, alignment, and avoidance are typically applied with the assumption that each individual has perfect knowledge of the position and orientation of its neighbors. However, this assumption may not hold true in practice, especially when some neighboring individuals are hidden from view [16–18]. As a result, it has been suggested that flocks of starlings might adjust their density to reach a state of “marginal opacity”, where the density of the group is sufficient to obscure individual positions without obstructing information transmission [19]. However, this density adjustment does not seem to be widespread, as certain animal groups such as fish schools can have much denser formations where individuals are not directly visible [10, 20].

In a recent study, Bastien and Romanczuk proposed a model of collective behavior based purely on visual information [21]. Instead of relying on relative positions and orientations, their model simulates each individual's response to a coarse-grained projection of its visual field. While they claim to use the simplest possible equations of movement that satisfy fundamental symmetries, their model involves six parameters that are hard to relate to the classical “3A” rules.

Here, we want to build an easily relatable collective behavior model inspired by animal vision, which incor-

porates the crucial role of the optic flow [22–24]. Optic flow refers to the apparent angular velocity of objects in the visual field due to the relative motion between the observer and the environment. The perception of an optic flow has been identified in various species, for instance, insects use it to navigate in cluttered environments [25], to avoid obstacles on the ground and to control the landing [26], fish use it to navigate [27], and even birds use during take off [28]. This natural perception has prompted researchers to develop algorithms and technologies that mimic this process, which has led to innovations in the fields of robotics [24, 29] and artificial vision [30, 31].

In this letter, we propose a model of collective behavior inspired by animal vision, which uses a coarse-grained optic flow as sensory input.

We consider a system of self-propelled particles in a two-dimensional environment, where each particle is represented as a circular object with radius a and moves with a constant speed U . The position of the i -th particle is \mathbf{x}_i , and its direction is indicated by a unit vector $\mathbf{e}_i = (\cos \theta_i, \sin \theta_i)$, where θ_i denotes its heading direction (Fig. 1a).

To model the visual perception of the individuals, we assume that each particle has access to its own visual field. Which is represented as the function $\mathcal{V}(\phi)$, where ϕ is the angle between the heading direction of the particle and the line of sight. The output of this function is binary, and represents the presence or absence of any object on the visual field (Fig. 1bc).

Using the information from the visual field $\mathcal{V}(\phi)$, we can calculate the function $\mathcal{R}(\phi) = a/\sin(\Delta\phi/2)$, where $\Delta\phi$ is the angle of vision of a shade. This function $\mathcal{R}(\phi)$ scales the visual field to self referred information, assuming that each shade corresponds to a single particle with a radius of a (Fig. 1d).

The temporal changes in the visual field $\mathcal{V}(\phi)$ can be used to calculate the optic flow $\mathcal{O}(\phi)$. Assuming that each shade has a pattern that moves and deforms with it, we estimate a coarse-grained version of the optic flow. Specifically, for each shade, $\mathcal{O}(\phi)$ is a linearly interpolated function of the angular velocity between the two

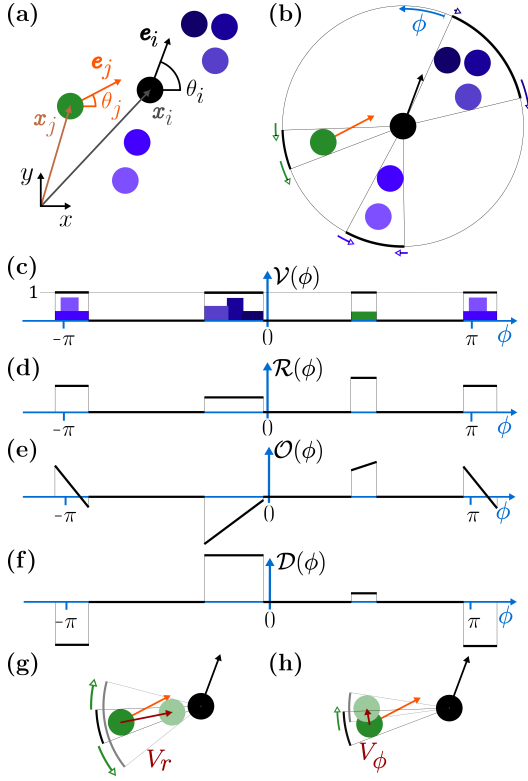


FIG. 1. Model notations and visual cues. (a) Snapshot of a group: \mathbf{x}_i is the position and θ_i the heading of the particle i . (b) Representation of the visual information, with ϕ the angle between the heading direction and the line of sight. (c) Visual field $\mathcal{V}(\phi)$ with binary output associated to the 2D representation in (b). (d) Associated function $\mathcal{R}(\phi)$ that estimates the distance of each shade assuming it is related to a single individual of radius a . (e) optic flow $\mathcal{O}(\phi)$ associated to the angular velocity of the shade edges. (f) Associated optic flow divergence $\mathcal{D}(\phi)$, derivative of the optic flow. (g) Illustration of the link between $\mathcal{D}(\phi)$ and the radial velocity V_r . (h) Same for the link between $\mathcal{O}(\phi)$ and the azimuthal velocity V_ϕ .

edges of the shade (Fig. 1e).

Note that this method for the optic flow calculation is akin to a cross-correlation of the visual field features: these feature-matching correlations [32] are known to be processed on animals eye [33, 34]. The optic flow \mathcal{O} incorporates more information than just using the derivative of the visual field \mathcal{V} [21].

We can also compute the optic flow divergence $\mathcal{D}(\phi)$ by taking the derivative of the optic flow $\mathcal{O}(\phi)$ (Fig. 1f). Due to the piece-wise linear nature of $\mathcal{O}(\phi)$, $\mathcal{D}(\phi)$ is a piece-wise constant function. As shown in Fig. 1gh, $\mathcal{D}(\phi)$ corresponds to the radial component V_r of the relative velocity between individuals, while the optic flow $\mathcal{O}(\phi)$ corresponds to the azimuthal component V_ϕ .

The optic functions \mathcal{V} , \mathcal{R} , \mathcal{O} , and \mathcal{D} are inspired by the way animals perceive their visual surroundings. These functions can also be easily computed by a man-made

system capable of rudimentary vision. We will see how to use these functions to construct a 3A model of attraction, alignment, and avoidance.

We model the interactions between particles using changes in their angular velocity associated with attraction/avoidance, alignment, and noise. Specifically, the equations of motion can be written as follows

$$\dot{\mathbf{x}}_i = U \mathbf{e}_i, \quad (1a)$$

$$\dot{\theta}_i = k_\circ \omega_\circ + k_\parallel \omega_\parallel + k_\eta \eta, \quad (1b)$$

where dots denote temporal derivatives, $\eta(t)$ is a standard Wiener process representing rotational noise, and k_\circ , k_\parallel , k_η are parameters that control the strength of attraction/avoidance, alignment, and noise, respectively. The functions ω_\circ and ω_\parallel are functions of order $O(1)$ associated with the visual cues.

The attraction term, denoted as ω_\circ , can be calculated from the visual field $\mathcal{V}(\phi)$ and the function $\mathcal{R}(\phi)$

$$\omega_\circ = \left\langle \int_{-\pi}^{\pi} \mathcal{V}(\phi) A(\mathcal{R}(\phi)) b_\epsilon(\phi) \sin \phi d\phi \right\rangle. \quad (2)$$

Here, the function $b_\epsilon(\phi) = 1 + \epsilon \cos \phi$ represents the blind spot of the visual field. When $\epsilon = 0$, b_ϵ is isotropic and there is no blind spot. When $\epsilon = 1$, the particle cannot see behind itself. In Eq. (2), A represents the transition from avoidance to attraction. We choose $A = -1$ (avoidance) for $\mathcal{R} < a$ and $A = 1$ (attraction) for $\mathcal{R} \geq a$. When $A = 1$, Eq. (2) describes an attraction towards the average line of sight of $\mathcal{V}(\phi)$, weighted by $b_\epsilon(\phi)$. The operator $\langle \cdot \rangle$ refers to the following normalization operation, which ensures that ω_\circ is of order 1

$$\left\langle \int f(\phi) \sin \phi d\phi \right\rangle = \int f(\phi) \sin \phi d\phi / \int |f(\phi)| d\phi. \quad (3)$$

To compute the alignment term ω_\parallel , which measures the misalignment of particles, we must estimate the cross products $\mathbf{e}_i \times \mathbf{e}_j$. This is done by using the optic flow $\mathcal{O}(\phi)$ and its divergence $\mathcal{D}(\phi)$, which are related to the two velocity components of particle j with respect to particle i (Fig. 1gh). Specifically, the radial component is given by $V_r = -\mathcal{R}(\phi) \mathcal{D}(\phi)$, and the azimuthal component by $V_\phi = \mathcal{R}(\phi) \mathcal{O}(\phi)$. We can use these components to calculate the heading vector \mathbf{e}_j in polar coordinates (r, ϕ) as $\mathbf{e}_j = (-\mathcal{D}, \mathcal{O})R(\phi)/U$, while \mathbf{e}_i can be expressed as $(\cos \phi, -\sin \phi)$.

We can now write the alignment term ω_\parallel as,

$$\omega_\parallel = \left\langle \int_{-\pi}^{\pi} (\mathbf{e}_i \times \mathbf{e}_j) b_\epsilon(\phi) d\phi \right\rangle, \quad (4)$$

which can be decomposed into radial and azimuthal components: $\omega_\parallel = \omega_{\parallel,r} + \omega_{\parallel,\phi}$, written as

$$\omega_{\parallel,r} = \left\langle \int_{-\pi}^{\pi} -\mathcal{D}(\phi) \mathcal{R}(\phi) b_\epsilon(\phi) \sin \phi d\phi \right\rangle / U, \quad (5a)$$

$$\omega_{\parallel,\phi} = \left\langle \int_{-\pi}^{\pi} \mathcal{O}(\phi) \mathcal{R}(\phi) b_\epsilon(\phi) \cos \phi d\phi \right\rangle / U. \quad (5b)$$

Here, $\langle \cdot \rangle$ denotes the normalization operation given by Eq. (3) (with the sine function replaced by cosine for $\omega_{\parallel, \phi}$). Note that the optic flow $\mathcal{O}(\phi)$ contains a component linked to the self-rotation of particle i . Therefore, we subtract $\dot{\theta}_i$ from $\mathcal{O}(\phi)$ before computing $\omega_{\parallel, \phi}$. Here, we use the relative velocity between particles, whereas most self-propelled-particle models use absolute velocities. However, in the present formulation, the two approaches are equivalent since $\mathbf{e}_i \times \mathbf{e}_j = \mathbf{e}_i \times (\mathbf{e}_j - \mathbf{e}_i)$.

The equations of motion presented in Eq. (1), along with the attraction and alignment terms derived in Eqs. (2) and (5), provide a model of collective behavior based on realistic visual cues. To make the problem dimensionless, we can use the particle radius and the Wiener process as characteristic scales of length and time, respectively, and set $a = 1$ and $k_\eta = 1$. By doing so, we obtain a dimensionless problem with four parameters for any simulation: U , k_\odot , k_\parallel , and ϵ . These parameters set the particle speed, the strength of attraction, the strength of alignment, and the blind angle, respectively.

Here, the visual field $\mathcal{V}(\phi)$ is a binary function: particles see other particles in black and white. Consequently, the visual functions \mathcal{V} , \mathcal{R} , \mathcal{O} , and \mathcal{D} are entirely characterized by a finite number of scalars, representing the positions and angular velocities of the shade edges. Leveraging this finite set, we can convert the continuous formulations of Eqs. (2) and (5) into a more efficient and discrete formulation (for practical implementation details, refer to [35][36]).

To investigate the impact of these parameters on collective behaviors, we conducted numerical simulations using a population of $N = 50$ randomly oriented particles initially placed in a circle of radius $aN/2$. We checked that the outcomes of the simulations were insensitive to these specific initial conditions. We numerically solved the dynamical system described by Eqs. (1–5) using an explicit scheme with a time step of $\delta t = 0.1$. We also examined the effect of the time step by conducting simulations with $\delta t = 0.001, 0.01, 0.1$, and 1 (SFig. 3–6 [35]). However, we observed no significant differences and opted to use $\delta t = 0.1$ as a good balance between resolution and computational efficiency.

We first set $U = 2$ and $\epsilon = 0$ (no blind angle) and examine the two remaining dimensionless parameters (k_\odot , and k_\parallel). Our simulations reveal three distinct dynamical phases (Fig. 2, and Supplementary Material for movies [35], SFig 7–9). When the strength of alignment is weaker than the noise ($k_\parallel \ll 1$), a disordered swarming phase emerges, where individuals form a sparse group without preferred orientation (Fig. 2a). As alignment strength increases, particles start to align in the same direction, leading to the schooling phase (Fig. 2b). When alignment and attraction are comparable and noise is low to moderate, the group exhibits a milling phase (Fig. 2c), where it forms a vortex. Interestingly, these three phases (swarming, schooling, and milling) have also been re-

ported in a self-propelled-particle model based on perfect knowledge of the positions and orientations of neighbors [8, 37–39].

To quantitatively distinguish between the different dynamical phases, we introduce three global order parameters: the polarization P , the milling M , and the normalized standard deviation S [37, 38]. These parameters are defined as follows,

$$P = \|\overline{\mathbf{e}_i}\|, \quad (6a)$$

$$M = \|\overline{\mathbf{y}_i \times \mathbf{e}_i}\|, \quad (6b)$$

$$S = \left(\overline{\|\mathbf{x}_i - \overline{\mathbf{x}_i}\|^2} / a^2 \right)^{1/2}, \quad (6c)$$

where the overbar denotes averaging over all individuals and $\mathbf{y}_i = (\mathbf{x}_i - \overline{\mathbf{x}_i}) / \|\mathbf{x}_i - \overline{\mathbf{x}_i}\|$ is the unit vector pointing towards the particle i from the center of mass of the group. The polarization P and the milling M both range between 0 and 1. A value $P = 0$ corresponds to a group with particles pointing in all directions, while $P = 1$ corresponds to a perfect school with all particles pointing in the same direction. The milling M represents the normalized angular momentum of the group. A straight-line formation results in $M = 0$, whereas a perfect milling phase results in $M = 1$. Finally, S is the normalized standard deviation and therefore reflects the average distance between individuals in the group.

To evaluate the role of attraction and alignment strengths, we ran a series of simulations, with three velocities ($U = 0.5, 2$, and 5), and two values of ϵ (0, indicating no blind angle, and 1, representing the maximum blind angle). For each parameter set, we obtained the values of P , M , and S by averaging over a period of $\Delta t = 100$ after waiting for 100 dimensionless time units to ensure the transient dynamics had settled. We performed ensemble averaging over 10 realizations and compiled the results in phase diagrams (Fig. 3).

Our vision-based model successfully reproduces the phases observed in traditional self-propelled-particle models, where individuals perfectly know the locations and orientations of their neighbors [15, 38, 40]. Specifically, we observe that for $P > 0.5$, the group exhibits a schooling phase, which occurs approximately when $k_\odot < k_\parallel$ (Fig. 3). For $M > 0.5$, the group enters a milling phase (for $k_\odot > k_\parallel$ and $k_\parallel > 0.3$ approximately). Conversely, for $M < 0.5$ and $P < 0.5$, we observe a swarming phase ($k_\parallel < 0.3$). These three phases form distinct regions in the (k_\parallel, k_\odot) space, which do not change qualitatively with varying velocity U or the blind angle parameter ϵ (Fig. 3).

However, we find that adding a blind angle tends to favor milling. Specifically, it extends the region of milling, and milling is more pronounced, as indicated by a larger value of M and a smaller value of P , compared to simulations without a blind angle. Interestingly, we also observe that the effect of a lower velocity is more pronounced with a blind angle, with a larger region of swarming in

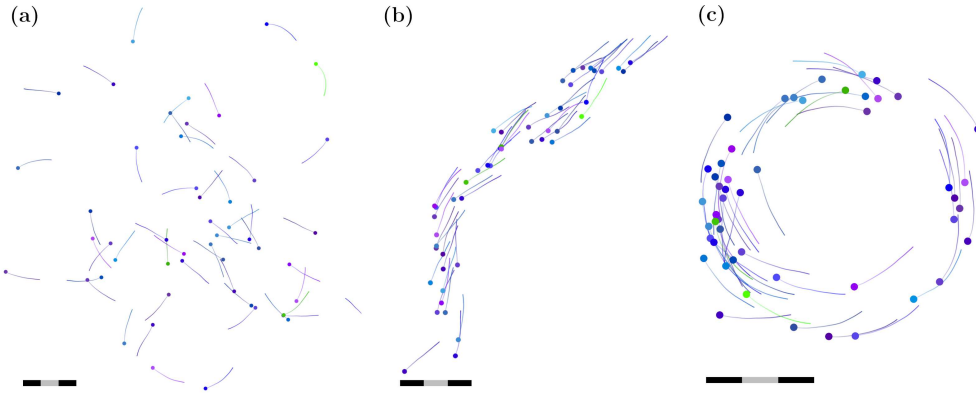


FIG. 2. Illustration of the phases observed for $N = 50$ individuals. There is no blind angle ($\epsilon = 0$) and the speed is $U = 2$. The scale bar measures $30a$ ($10a$ for each section). We observe three phases: (a) swarming ($k_{\odot} = 2$, $k_{\parallel} = 0$); (b) schooling ($k_{\odot} = 1.5$, $k_{\parallel} = 2$); (c) milling ($k_{\odot} = 2$, $k_{\parallel} = 1.5$).

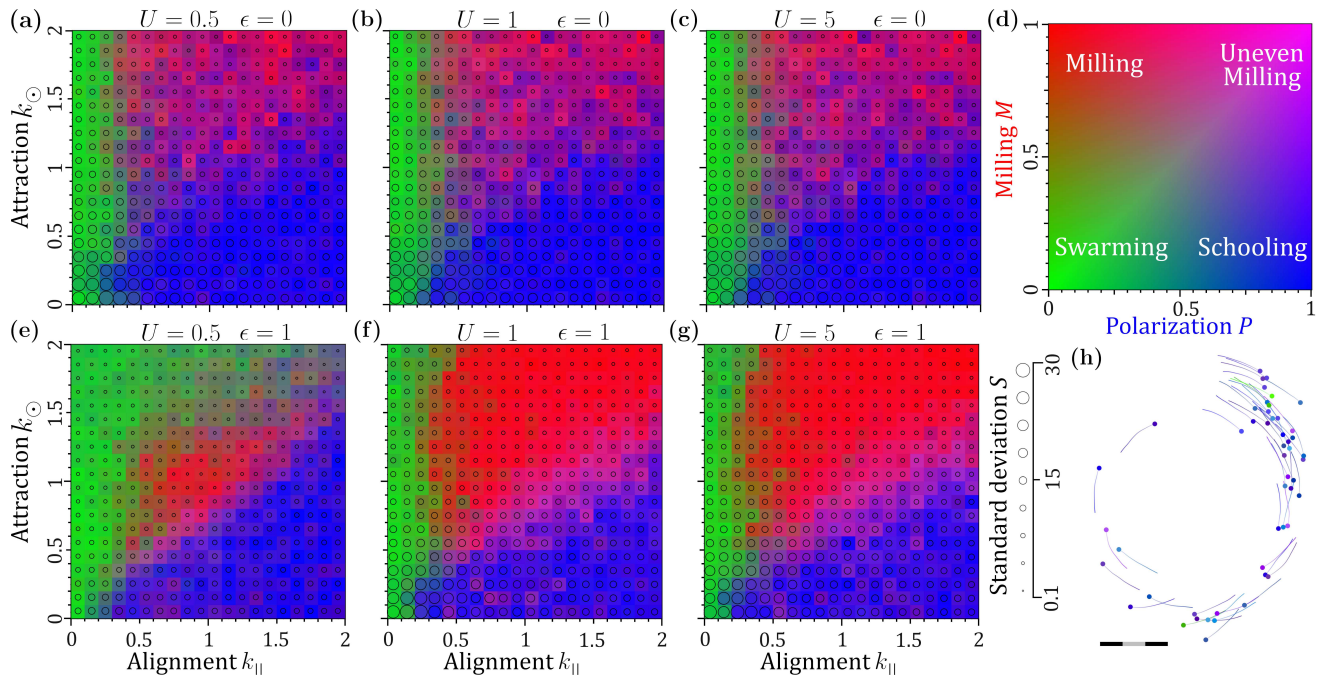


FIG. 3. Phase diagrams for 50 individuals. For (a-c), there is no blind angle ($\epsilon = 0$), for (e-g), the blind angle is maximum ($\epsilon = 1$). Each column corresponds to a different speed: $U = 0.5$ (a, e); $U = 2$ (b, f); and $U = 5$ (c, g). In the phase space (k_{\parallel}, k_{\odot}), each color represents different values of P and M as illustrated in the colormap (d). An uneven milling phase can be observed for some values of the parameters: $U = 5$, $\epsilon = 1$, $k_{\parallel} = 1.5$, $k_{\odot} = 1$ (h).

the phase diagram for $U = 0.5$ (Fig. 3e) compared to other velocities. This effect is not observed in simulations without a blind angle.

Classical models do not typically exhibit milling behavior in the absence of a blind angle [37, 38], but in our model, we observe milling probably due to visual obstructions acting as a substitute for the blind angle. However, the resulting milling behavior we observe is often uneven, as illustrated in Fig. 3h. Additionally, we observe intermittent transitions between schooling and milling, which may account for the poor reproducibility of P and M

values in the milling region of the phase diagrams (Fig. 3a-c), especially when $\epsilon = 0$.

To investigate the effect of group size on our results, we examined the milling phase for flocks of varying sizes, ranging from 10 to 300 individuals having a visual blind angle (Fig. 4). Using the same set of parameters ($k_{\odot} = 2$, $k_{\parallel} = 2$, $U = 2$, and $\epsilon = 1$), we observed that most groups first expanded and then contracted to reach a stable density, with a value of $S \approx 20$. Note, for large flocks ($N > 300$) the group does several swirls (see SFig 16 and SVideo 14), which generate the oscillations of P

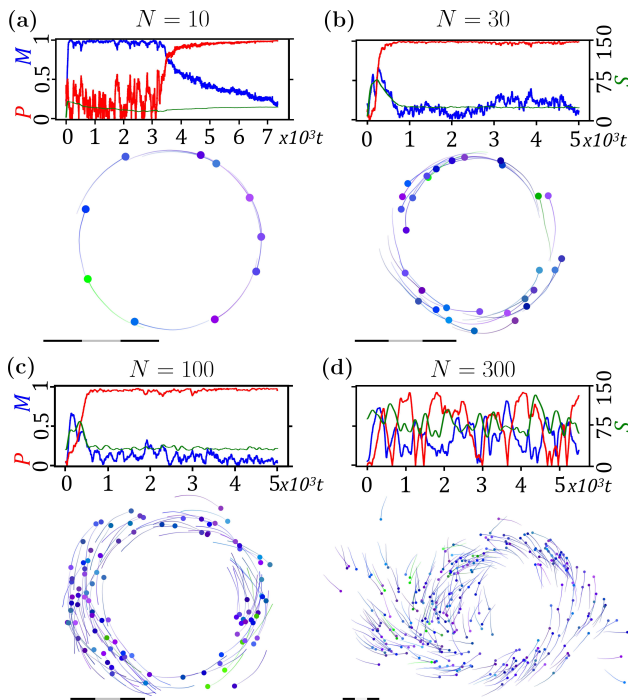


FIG. 4. Effect of group size on the milling phase. We use the same parameters ($U = 2, k_{\odot} = 2, k_{\parallel} = 2$ and $\epsilon = 1$) and four group sizes: $N = 10$ (a); $N = 30$ (b); $N = 100$ (c); and $N = 300$ (d). Together with an illustration of the group are plotted the evolution of the phase parameters P (blue), M (red), and S (green).

and M , seen on Fig. 4d. During this process, we observed a local maximum in the polarization P , followed by a decrease to almost zero, while the milling M increased monotonously to reach a value close to 1.

Our results, presented in Fig. 4 (see also Supplementary Material for movies [35]), indicate that group size N has a negligible effect on the phases observed. This is surprising given that many models exhibit an effect of group size. However, we hypothesize that the normalization used to define the attraction and alignment rules, as given by Eq. (3), may play a role in preserving the observed phases regardless of group size.

In our vision-based model, the radius of the particle plays an important role. This is the only quantity that sets the standard deviation S in the simulations, since the attraction and alignment rules are otherwise scale-free. As seen in Fig. 4, the standard deviation S converges to a steady value for given attraction and alignment strengths, but this value does not seem to depend strongly on the group size. This suggests that vision sets a certain volume fraction, and not the opacity as previously suggested [19].

In conclusion, our model of collective behavior based only on a coarse-grained optic flow, a bioplausible visual cue, successfully reproduces swarming, schooling, and milling, which are the three classical collective behaviors

observed in animal groups. This work shows that realistic visual information alone can be used to construct a model of collective animal behavior. This suggests a new approach to modeling the dynamics of animal groups.

Moreover, our findings suggest potential applications for coordinating swarms of artificial drones, which could be controlled using similar visual cues. In future work, we plan to explore these possibilities further and refine our model to better capture the complexity and richness of real-world animal group behavior in three dimensions.

* diego-mauricio.castro-rondon@univ-amu.fr

- [1] B. Liebchen and D. Levis, Collective behavior of chiral active matter: Pattern formation and enhanced flocking, *Physical Review Letters* **119**, 058002 (2017).
- [2] J.-B. Caussin, A. Solon, A. Peshkov, H. Chaté, T. Dauxois, J. Tailleur, V. Vitelli, and D. Bartolo, Emergent spatial structures in flocking models: a dynamical system insight, *Physical Review Letters* **112**, 148102 (2014).
- [3] L. Barberis and F. Peruani, Large-scale patterns in a minimal cognitive flocking model: incidental leaders, nematic patterns, and aggregates, *Physical Review Letters* **117**, 248001 (2016).
- [4] J. L. Silverberg, M. Bierbaum, J. P. Sethna, and I. Cohen, Collective motion of humans in mosh and circle pits at heavy metal concerts, *Physical Review Letters* **110**, 228701 (2013).
- [5] T. Vicsek, A. Czirók, E. Ben-Jacob, I. Cohen, and O. Shochet, Novel type of phase transition in a system of self-driven particles, *Physical Review Letters* **75**, 1226 (1995).
- [6] S. Martin, Multi-agent flocking under topological interactions, *Systems & Control Letters* **69**, 53 (2014).
- [7] D. S. Calovi, A. Litchinko, V. Lecheval, U. Lopez, A. Pérez Escudero, H. Chaté, C. Sire, and G. Theraulaz, Disentangling and modeling interactions in fish with burst-and-coast swimming reveal distinct alignment and attraction behaviors, *PLoS computational biology* **14**, e1005933 (2018).
- [8] X. Lu, C. Zhang, and B. Qin, An improved vicsek model of swarm based on remote neighbors strategy, *Physica A: Statistical Mechanics and its Applications* **587**, 126553 (2022).
- [9] C. W. Reynolds, Flocks, herds and schools: A distributed behavioral model, in *Proceedings of the 14th annual conference on Computer graphics and interactive techniques* (1987) pp. 25–34.
- [10] F. Ginelli and H. Chaté, Relevance of metric-free interactions in flocking phenomena, *Physical Review Letters* **105**, 168103 (2010).
- [11] E. V. Albano, Self-organized collective displacements of self-driven individuals, *Physical Review Letters* **77**, 2129 (1996).
- [12] Y. Katz, K. Tunström, C. C. Ioannou, C. Huepe, and I. D. Couzin, Inferring the structure and dynamics of interactions in schooling fish, *Proceedings of the National Academy of Sciences* **108**, 18720 (2011).
- [13] S. Mishra, A. Baskaran, and M. C. Marchetti, Fluctuations and pattern formation in self-propelled particles,

- Physical Review E **81**, 061916 (2010).
- [14] A. P. Solon, J.-B. Caussin, D. Bartolo, H. Chaté, and J. Tailleur, Pattern formation in flocking models: A hydrodynamic description, *Physical Review E* **92**, 062111 (2015).
- [15] T. Vicsek and A. Zafeiris, Collective motion, *Physics reports* **517**, 71 (2012).
- [16] E. Soria, F. Schiano, and D. Floreano, The influence of limited visual sensing on the reynolds flocking algorithm, in *2019 Third IEEE International Conference on Robotic Computing (IRC)* (IEEE, 2019) pp. 138–145.
- [17] J. D. Davidson, M. M. Sosna, C. R. Twomey, V. H. Sridhar, S. P. Leblanc, and I. D. Couzin, Collective detection based on visual information in animal groups, *Journal of the Royal Society Interface* **18**, 20210142 (2021).
- [18] A. Strandburg-Peshkin, C. R. Twomey, N. W. Bode, A. B. Kao, Y. Katz, C. C. Ioannou, S. B. Rosenthal, C. J. Torney, H. S. Wu, S. A. Levin, *et al.*, Visual sensory networks and effective information transfer in animal groups, *Current Biology* **23**, R709 (2013).
- [19] D. J. G. Pearce, A. M. Miller, G. Rowlands, and M. S. Turner, Role of projection in the control of bird flocks, *Proceedings of the National Academy of Sciences* **111**, 10422 (2014).
- [20] Y. Shang and R. Bouffanais, Influence of the number of topologically interacting neighbors on swarm dynamics, *Scientific reports* **4**, 1 (2014).
- [21] R. Bastien and P. Romanczuk, A model of collective behavior based purely on vision, *Science advances* **6**, eaay0792 (2020).
- [22] F. Ruffier and N. Franceschini, Optic flow regulation: the key to aircraft automatic guidance, *Robotics and Autonomous Systems* **50**, 177 (2005).
- [23] L. Bergantin, N. Harbaoui, T. Raharijaona, and F. Ruffier, Oscillations make a self-scaled model for honeybees’ visual odometer reliable regardless of flight trajectory, *Journal of the Royal Society Interface* **18**, 20210567 (2021).
- [24] G. C. De Croon, J. J. Dupeyroux, C. De Wagter, A. Chatterjee, D. A. Olejnik, and F. Ruffier, Accommodating unobservability to control flight attitude with optic flow, *Nature* **610**, 485 (2022).
- [25] G. Portelli, F. Ruffier, and N. Franceschini, Honeybees change their height to restore their optic flow, *Journal of Comparative Physiology A* **196**, 307 (2010).
- [26] N. Franceschini, F. Ruffier, and J. Serres, A bio-inspired flying robot sheds light on insect piloting abilities, *Current Biology* **17**, 329 (2007).
- [27] K. Bonnen, Motion vision: Fish swimming to see, *Current Biology* **33**, R30 (2023).
- [28] J. R. Serres, T. J. Evans, S. Åkesson, O. Duriez, J. Shamoun-Baranes, F. Ruffier, and A. Hedenström, Optic flow cues help explain altitude control over sea in freely flying gulls, *Journal of The Royal Society Interface* **16**, 20190486 (2019).
- [29] F. Expert and F. Ruffier, Flying over uneven moving terrain based on optic-flow cues without any need for reference frames or accelerometers, *Bioinspiration & biomimetics* **10**, 026003 (2015).
- [30] D. Floreano, R. Pericet-Camara, S. Violette, F. Ruffier, A. Brückner, R. Leitel, W. Buss, M. Menouni, F. Expert, R. Juston, M. K. Dobrzynski, G. L’Eplattenier, F. Recktenwald, H. A. Mallot, and N. Franceschini, Miniature curved artificial compound eyes, *Proceedings of the National Academy of Sciences* **110**, 9267 (2013).
- [31] F. Schilling, E. Soria, and D. Floreano, On the scalability of vision-based drone swarms in the presence of occlusions, *IEEE Access* **10**, 28133 (2022).
- [32] H. Ullman, Analysis of visual motion by biological and computer systems, *Computer* **14**, 57 (1981).
- [33] N. Franceschini, A. Riehle, and A. Le Nestour, Directionally selective motion detection by insect neurons, in *Facets of vision* (Springer, 1989) pp. 360–390.
- [34] H. Eichner, M. Joesch, B. Schnell, D. F. Reiff, and A. Borst, Internal structure of the fly elementary motion detector, *Neuron* **70**, 1155 (2011).
- [35] Supplemental material resources of this paper.
- [36] The open source code will be available when the paper is accepted.
- [37] D. S. Calovi, U. Lopez, S. Ngo, C. Sire, H. Chaté, and G. Theraulaz, Swarming, schooling, milling: phase diagram of a data-driven fish school model, *New journal of Physics* **16**, 015026 (2014).
- [38] A. Filella, F. Nadal, C. Sire, E. Kanso, and C. Eloy, Model of collective fish behavior with hydrodynamic interactions, *Physical Review Letters* **120**, 198101 (2018).
- [39] H. J. Charlesworth and M. S. Turner, Intrinsically motivated collective motion, *Proceedings of the National Academy of Sciences* **116**, 15362 (2019).
- [40] C. Kolon and I. B. Schwartz, The dynamics of interacting swarms (2018), arXiv:1803.08817.